

# Dimensional Reduction for Single Molecule Imaging of DNA and Nucleosome Condensation by polyamines, HP1 $\alpha$ and Ki-67

Nils A. Benning <sup>a</sup>, Jacob Kæstel-Hansen <sup>b</sup>, Fahad Rashid <sup>c</sup>, Sangwoo Park <sup>c</sup>, Raquel Merino Urteaga <sup>a</sup>, Ting-Wei Liao <sup>c</sup>, Jingzhou Hao <sup>c</sup>, James M. Berger <sup>c</sup>, Nikos S. Hatzakis <sup>b, d</sup>, Taekjip Ha <sup>a, c, e, f, \*</sup>

<sup>a</sup> Department of Biophysics, Johns Hopkins University, Baltimore, MD 21218, USA

<sup>b</sup> Department of Chemistry and Nanoscience Centre, University of Copenhagen, Copenhagen, Denmark

<sup>c</sup> Department of Biophysics and Biophysical Chemistry, Johns Hopkins University School of Medicine, Baltimore, MD 21205, USA

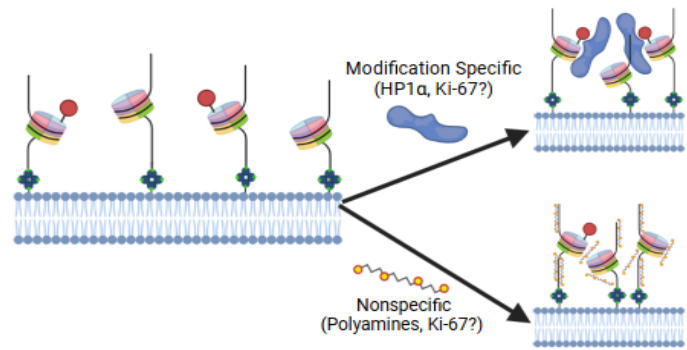
<sup>d</sup> Novo Nordisk Foundation Centre for Protein Research, Faculty of Health and Medical Sciences, University of Copenhagen, Copenhagen, Denmark

<sup>e</sup> Department of Biomedical Engineering, Johns Hopkins University, Baltimore, MD 21218, USA

<sup>f</sup> Howard Hughes Medical Institute, Baltimore, MD 21205, USA

\*email: tjha@jhu.edu

**ABSTRACT:** Macromolecules organize themselves into discrete membrane-less compartments through a process called liquid-liquid phase separation (LLPS). Mounting evidence has suggested that nucleosomes as well as DNA itself undergo LLPS or general condensation to regulate genomic activity. Current in vitro condensation studies provide insight into the physical properties of condensates, such as surface tension and diffusion. However, such studies lack the resolution that would allow for complex kinetic studies of multicomponent condensation. To address this issue, we use a supported lipid bilayer (SLB) platform in tandem with objective based total internal reflection microscopy (TIRM) to observe the 2-dimensional lateral movement of macromolecules at single-molecule resolution. This dimensional reduction from 3-dimensional studies allows us to observe the initial condensation events of DNA and nucleosomes and dissolution of these early condensates in the presence of condensing agents at physiological concentrations. We observe that the initial condensation of DNA and nucleosomes happens on a timescale of minutes while dissolution occurs within seconds. Specifically, we used this platform to observe polyamine-mediated DNA condensation. Polyamines are found in abundance in some condensate related diseases, such as Alzheimer's and various cancers. Our real-time imaging of condensation verified that polyamine valency directly impacts DNA as well as nucleosome condensability, in line with previous finding that polycations interact with the negatively charged DNA backbone. Lastly, we use this platform to study nucleosome condensing agents, such as HP1 $\alpha$  and Ki-67 to observe their effects on promoting condensation.



**KEYWORDS:** *Supported Lipid Bilayer (SLB), Spermine, HP1 $\alpha$ , Ki-67, Particle Tracking, Diffusion, Nucleosome*

## 1. INTRODUCTION

A resurgent concept in biology is the way cells organize biomolecules into membrane-less compartments through LLPS. This organization of biomolecules facilitates cellular reactions once their concentration reaches a certain threshold. These biomolecular condensates exist in the nucleus to facilitate processes, such as DNA damage repair, gene repression through chromatin condensation, and ribosome biogenesis [2-4], and in the cytosol to facilitate mRNA processing, mRNA localization, translation, protein folding, along with many other processes [5]. Because LLPS is involved in many cellular functions, it must be highly regulated. Dysregulation of LLPS may result in the formation of pathological aggregates that lead to impaired cell function and may ultimately lead to cell death [5-15], highlighting the importance of understanding the tight regulation of LLPS in cells.

LLPS is promoted through interactions between macromolecules and depends on valency of interactions. Many proteins associated with LLPS achieve multivalency through the interaction of two

generally conserved modules: folded domains and low complexity disordered segments [5,2,16]. Entropy typically favors a heterogeneous mixture and is governed by environmental factors like pH and temperature, but many biological condensates circumvent this through multivalent interactions between different constituents. These multivalent interactions can promote organized compartmentalization of subcellular components as seen in nucleolar organization [4]. LLPS is also dependent on the concentration threshold of macromolecules where a critical concentration must be reached for macromolecules to undergo phase separation. While advances in the field detail the types of multivalent interactions and potential critical concentrations of phase separating proteins that promote LLPS, there is still more to learn about the selective concentrating of LLPS promoting molecules for cellular processes that involve these proteins [17,18]. In addition, while live-cell based studies have been performed using a protein construct with tunable valency [19,20], many do not capture kinetic rates efficiently at a single molecule level.

Single molecule studies provide enhanced resolution to observe the kinetics of condensate formation and macromolecule recruitment into a condensate [21, 22, 52, 53]. Here, we used a supported lipid bilayer (SLB) to investigate 2-dimensional lateral movement of DNA and nucleosome condensation at a single-molecule level. Such SLBs have been used to study vesicle fusion as well as cell adhesion [23, 24, 47, 48, 49], and, importantly, the clustering of components within the bilayer like individual lipids and cholesterol [25]. This platform allows us to correlate the kinetic behavior of SLB-bound molecules with their condensate properties and can also be applied to investigating the recruitment kinetics of other phase separating proteins or macromolecules. One protein of particular interest is Ki-67, a 2896 amino acid protein that coats mitotic nucleosomes to maintain chromosomes individuality during mitosis after the mitotic envelope dissociates [30]. At the end of mitosis, Ki-67 aids in the exclusion of cytoplasm during the reformation of the nuclear envelope. Such condensation is essential for Ki-67s functioning in vivo. Thus, understanding how Ki-67 operates as a chromosomal condensing agent could serve to help us better understand general nucleosome organization as well as what role Ki-67 overexpression plays as ubiquitous proliferation marker for multiple types of cancer.

## 2. METHODS

### 2.1 Supported lipid bilayer (SLB) generation

SLBs were generated based on studies that observe vesicle fusion into bilayers [23]. Small unilamellar vesicles are prepared by drying a mixture of 93% POPC and 7% 18:1 biotinyl-PE (Avanti Polar Lipids, catalog #850457C and 870282C) under compressed nitrogen gas followed by overnight drying under vacuum. This “lipid cake” was hydrated with T50 Buffer (10mM Tris-HCL pH 8.0, 50 mM NaCl) and pipetted several times to promote vesicle formation. After undergoing 15 freeze-thaw cycles using liquid nitrogen, small unilamellar vesicles (SUVs) were prepared by 21 passes through an extruder (Avanti) fitted with 100 nm filter (Cytiva, catalog # 800309). SUVs were stored at 4°C for up to 14 days.

### 2.2 Slide Preparation/Assembly

Quartz slides were cleaned by sonicating in methanol for 30 min, then washing with acetone and drying with nitrogen gas. After drying, the slides were sonicated in a 5% Alconox detergent solution for 30 min and rinsed with ddH<sub>2</sub>O. Slides were then sonicated in a 1 M KOH solution, rinsed with ddH<sub>2</sub>O, and burned using a propane torch. Glass coverslips were incubated in a 1X detergent solution (MP Biomedicals, 097667093) just below boiling point for 1 hour and then thoroughly rinsed with MilliQ water. Glass coverslips were then baked in a Furnace (Barnstead International, Model FB1315M) at 540 °C, just below the melting point of the coverslip, for 5 hours. Once clean, 1-2 mm strips of Scotch double-sided tape were placed between drilled holes on the edges of the quartz slide. The glass coverslips were then briefly burned using a propane torch and placed on the tape covered quartz slide. Excess tape was removed, and the edges of the slide were sealed using epoxy (Devcon), resulting in a final assembled reaction chamber. Functional imaging slides are made by injecting 20 µL of SUVs into a reaction chamber for 30 minutes incubating for vesicle fusion and SLB formation. The excess free SUVs were then washed out with 200 µL of T50 Buffer.

### 2.3 oTIRF microscopy/ Analysis

Fluorescently labeled macromolecules (DNA and mononucleosomes) were observed on the SLBs using objective-based total internal reflection fluorescence microscopy. The fluorescence emission was collected by oil objective (Nikon PlanApo, NA 1.40, 60×) and recorded by a back-illuminated electron-multiplying charge-coupled device camera (iXon3, Andor Technology) with 50 ms exposure time.

To measure initial condensation, several criteria were put in place to define a potential condensate where a minimum of two criteria must be met: no diffusion, an intensity value at least double that of individual particles, and increased size relative to individual particles. Once a potential condensate is identified other potential condensates must also be easily located using the same criteria. When potential condensates are easily found (through random search) or multiple condensates appear within one field of view, initial condensation has occurred.

Single-molecule tracking was performed using the ImageJ plugin, TrackMate, with a Laplacian of Gaussian (LoG) filter detector, which enables analysis of merging and splitting events. XY coordinates were obtained from these videos for each particle in each frame, and trajectories for each particle were analyzed using a Linear Assignment Problem (LAP) tracker [26]. Diffusion coefficients for each particle were determined using a mean squared displacement (MSD) analysis. Trajectories were excluded based on trajectory length, where short trajectories (fewer than 10 frames) indicated particles that transiently entered the field of view. To investigate temporal changes in diffusional behavior we utilized rolling MSD analysis by fitting  $MSD = 2dDt^\alpha$ , where D is the diffusional coefficient,  $\alpha$  is a measure of persistence in the walk and d is the dimension. For the analysis we utilized a window size of 20, required restricted segment length to be > 10 timepoints to disregard spurious transient restricted movement and applied a system-specific threshold for restricted motion of  $MSD = 0.05 \mu m^2/s \cdot s^\alpha$ .

### 2.4 Widefield microscopy/ Analysis

Bulk diffusion measurements were obtained by preparing SLBs as described above and imaging via a 555nm excitation laser with a Cy3 emission filter using a water/oil-immersion objective (Nikon PlanApo  $\lambda$ , NA 0.75, 20x). FRAP experiments were performed using this microscope with a 50 mW bleaching laser at 405 nm and a Bruker Galvano mirror scanner. Regions of interest measuring 25 pixels in diameter on the SLB were bleached using 50% laser intensity for 1 second. Fluorescence recovery data was obtained immediately after bleaching and every 5 seconds up to 5 minutes.

### 2.5 Protein Purification and Nucleosome assembly

HP1 $\alpha$  was purified as described previously [50].

Mononucleosomes were generated as described previously [51] using human histones.

Full length Ki-67 gene was synthesized (Twist Bioscience) and inserted into the yeast expression plasmid (-Ura) along with N-terminal hexa histidine tag by Gibson assembly. Ki-67 was expressed in the *S. cerevisiae* strain BCY123. Starter cultures were grown to saturation overnight in CSM-Ura- media supplemented with 2% dextrose, 2% lactic acid, and 1.5% glycerol at 30 °C. Starter cultures were then diluted 10-fold in YP media with 2% lactic acid and 1.5% glycerol, and grown to an OD of 1.0–1.3 at 30 °C (12–15 h), at which point protein expression was induced by the addition of 2% galactose for 6 h at 30 °C. Cells were harvested by centrifugation, resuspended in 1 ml of 1 mM EDTA and 250 mM NaCl per liter of culture, and flash frozen dropwise in liquid nitrogen for storage at –80 °C.

For purification, frozen pellets were lysed by cryogenic grinding in a Freezer Mill (SPEX SamplePrep). The cell powder was resuspended in K-Buffer (50 mM HEPES-KOH (pH 7.5), 300 mM NaCl, 30 mM imidazole (pH 8.0), 10% glycerol, 1 mM PMSF, 2.34 µM leupeptin, 1.45 µM pepstatin, and 0.5 mM TCEP). Lysate was clarified by centrifugation at 16,000 rpm in a JA 25.50 rotor for 45 min and loaded onto a HisTrap HP (GE) nickel-chelating Sepharose column. Protein was eluted in K-Buffer with 250mM NaCl and 500mM Imidazole. Ki67 fractions were loaded onto Hitrap-SP column and eluted with K-buffer containing 1M NaCl. Fractions

containing Ki-67 was concentrated and loaded onto Superose6 10/300gl column pre-equilibrated in Storage buffer (50 mM Hepes-KOH (pH 7.5), 300 mM NaCl, 10% glycerol, 1mM TCEP). Fractions containing Ki-67 were pooled, concentrated and stored in -80C.

## 2.6 DNA synthesis

DNA was synthesized from a Widom 601 sequence containing plasmid pGEMz\_601 (Addgene, 26656) with primers containing a biotin and Cy3.

AT-rich, GC-rich, and all primers were constructed by IDT:

125bp AT-rich DNA

5'-  
AGCGGTGATGCTGATAGAAGTATAATATTAATAATAAA  
TTAAATATATTATTAATAATAATAAT  
TAATAAATTAATAATTTATAATAATTAACATAAT  
AGCTTCTGTGCGCC - 3'

122bp GC-rich DNA

5'  
TGAACCTGTACCCCTTGTGGCGCGTACGCGCAACGCGT  
TATCGTTCGCGTACGCGCGACGCGACGCGGATCGCGAA  
CGCGGTCGTGCGCGACGCGGCGCTTGTAGATGAAC  
TTGCG - 3'

70bp DNA (-77N0)

5' -  
CGTACGTGCGTTTAAAGCGGTGCTAGAGCTGTCTACGACC  
AATTGAGCGGCCTCGGCACCGGGATTCTCCA - 3'

147bp DNA (0N0)

5' -  
CAGGATGTATATATCTGACACGTGCCTGGAGACTAGGG  
AGTAATCCCCTTGGCGGTTAAAACGCGGGGGACAGCGC  
GTACGTGCGTTTAAAGCGGTGCTAGAGCTGTCTACGACCA  
ATTGAGCGGCCTCGGCACCGGGATTCTCCA - 3'

231bp DNA (43N43)

5' -  
ACTATCCGACTGGCACCGGCAAGGTCGCTGTTCAATACA  
TGCACAGGATGTATATATCTGACACGTGCCTGGAGACTA  
GGGAGTAATCCCCTTGGCGGTTAAAACGCGGGGGACAG  
CGCGTACGTGCGTTTAAAGCGGTGCTAGAGCTGTCTACGA  
CCAATTGAGCGGCCTCGGCACCGGGATTCTCCAGGGCG  
GCCGCGTATAGGGTCCATCACATAAGGGATGAACTCGG  
- 3'

## 3. RESULTS AND DISCUSSION

3.1 SLBs provide a platform for measuring fluid properties and LLPS at a single molecule level

Supported lipid bilayers (SLBs) are a widely used platform that mimics the cellular membrane. SLBs can be integrated into many surface-based techniques and have been useful for investigating fundamental phenomena in many fields, including membrane biology,

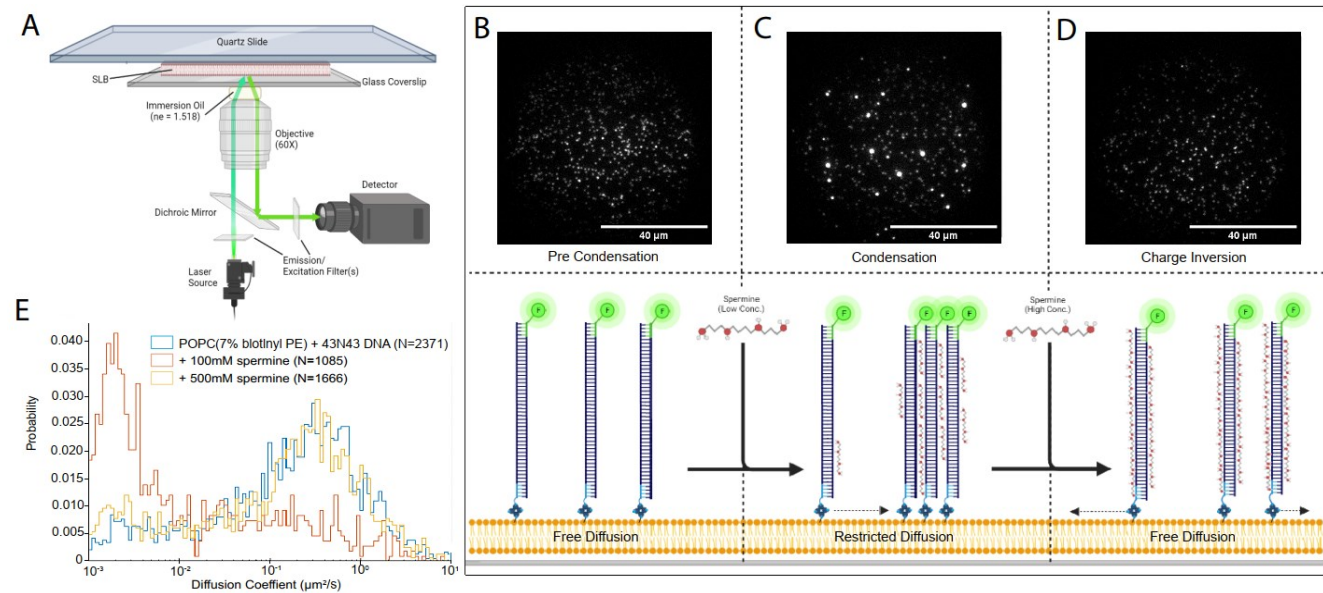


**Figure 1.** Experimental setup for experiments using objective-based total internal reflection fluorescence (oTIRF) microscopy in tandem with SLBs to observe spermine mediated condensation and decondensation: (A) oTIRF microscope setup, (B) visual representation and oTIRF recording of DNA bound to a 7% biotin containing SLB before the addition of any condensing agent, (C) visual representation and oTIRF recording of DNA bound to a 7% biotin containing SLB after promoting condensate formation through the addition of 100mM spermine, (D) visual representation and oTIRF recording of DNA bound to a 7% biotin containing SLB after inducing charge inversion and condensate dispersal through the addition of 500mM spermine, (E) diffusion histogram showing before, during, and after spermine mediated condensation and charge inversion of 40N40 DNA.

medical, and biotechnical fields [23, 24, 25]. Recent work has shown that SLBs are a suitable platform for investigating membrane bound liquid-liquid phase separation (LLPS), highlighting how traditional LLPS studies such as circular droplet formation,

fusion, and fluorescence recovery after photobleaching (FRAP) can be replicated in two dimensions [27].

As a proof of concept, we first formed SLBs containing 94% POPC, 1% 18:1 rhodamine PE for SLB visualization, and 5%

phosphatidylethanolamine mimic containing a biotinylated head group, 18:1 Biotinyl PE, and bound a biotin-labeled double stranded 43N43 DNA (where N denotes the 147bp 601 Widom positioning sequence and the adjacent numbers represent the linker DNA bp length) to the SLB through an avidin linkage. After the SLB was formed and DNA was bound, widefield imaging was performed to confirm the fluorescence homogeneity across the surface of the SLB (Supplemental Figure 1A). This was directly compared to an SLB containing 1% 18:1 rhodamine PE (99% POPC). A small area was selectively photobleached and fluorescence recovery was observed with a halftime of 65 s for the DNA-bound SLB and 69 s for the SLB with no bound DNA (Supplemental Figure 1B). From FRAP curves generated by the fluorescence recovery we determined the bulk diffusion coefficient of  $0.59 \pm 0.046 \mu\text{m}^2/\text{s}$  for 18:1 rhodamine PE containing SLBs and  $0.55 \pm 0.044 \mu\text{m}^2/\text{s}$  for 18:1 rhodamine PE-containing, DNA-bound SLBs. This indicates that the binding of DNA has little impact on the diffusion of lipids an SLB. These values are consistent with the diffusion coefficients of SLBs with membrane bound molecules determined in other studies [21, 48, 49].

By reducing the concentration of fluorescent molecules bound to the SLB, we could observe single molecule diffusion across the SLB surface using objective-based TIRF (Fig 1A). This allows for the tracking of individual particles at a particle density high enough for small condensates to form (Fig 1B, 1C). In order to test the efficacy of SLBs as a platform for observing condensation, we first bound a 230 base pair (bp) long DNA labeled with Cy3 to an SLB and were able to observe the lateral movement of particles with a diverse population of diffusion coefficients (Fig 1B, 1E). We then added 100 mM spermine, a 4+ charged polyamine, which has been shown to bridge adjacent DNA duplexes [28], to promote

condensate formation. After the addition of spermine, small condensates formed from smaller, dimmer particles (Fig 1C, 1E). In addition to the immobile condensates, we also observed mobile particles as well as individual particles with arrested movement. The population of mobile particles is likely dependent on the concentration of condensing agent and the type of condensing agent: charged based condensation as in the case of spermine eventually leads to charge inversion-mediated condensate dispersal and therefore likely has a window of concentration range where all particles are immobile. Condensate formation on SLB-bound particles relies on the lateral movement of phospholipids within the bilayer, where disruption of this movement could potentially lead to apparent condensation by irreversible membrane deformation and destruction. To rule out this possibility, we induced charge inversion by increasing the concentration of spermine to 500 mM, where the negatively charged DNA backbones become coated in positive charge from spermine. The resulting charge inversion is observed as dispersal of condensates previously formed by spermine (Fig 1D, Video1). Indeed, when using SLBs to observe spermine-mediated condensation and charge inversion, mobility of the surface bound particles recovers to levels before the addition of spermine (Fig 1D, 1E).

In this study, ‘initial condensation’ is described as the formation of bright, immobile puncta early when many particles are still mobile, and ‘definitive condensation’ is defined by a near complete loss of particle mobility and the ubiquitous formation of bright, immobile puncta (Fig 2A). We first varied the GC-content of DNA on condensation of densely populated DNAs on an SLB. AT-rich DNA initially condensed after the introduction of 5  $\mu\text{M}$  spermine, followed by 20  $\mu\text{M}$  spermine for DNA with 57% GC content, and 30  $\mu\text{M}$  for GC-rich DNA (Table 1). Titration points of 1  $\mu\text{M}$ , 10  $\mu\text{M}$ ,

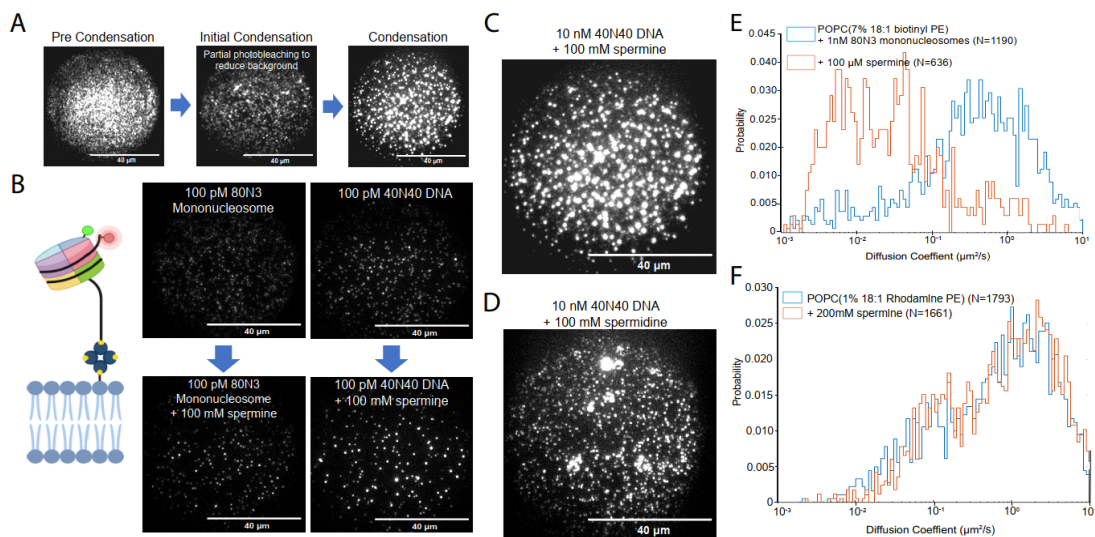


**Figure 2.** Condensation landscape: (A) definitions associated with condensation as they’re used in downstream experiments, (B) 80N3 mono-nucleosome construct used in future experiments, example recordings of 80N3 nucleosomes and 40N40 DNA before and after condensate formation by spermine. (C) SLB populated densely with DNA in the presence of spermine. (D) SLB populated densely with DNA in the presence of spermidine. (E) diffusion histogram showing before, and after spermine mediated condensation of 80N3 nucleosomes, (F) diffusion histogram of a noncondensing particle (Rhodamine conjugated lipid) in an SLB.

and 20  $\mu\text{M}$  spermine did not result in the initial condensation of AT-rich, 57% GC content, and GC-rich DNA, respectively.

DNA Length (bp)	Spermine (4+)
70	50 $\mu\text{M}$
147	20 $\mu\text{M}$

230	10 $\mu\text{M}$
AT-rich (125bp)	5 $\mu\text{M}$
GC-rich (125bp)	30 $\mu\text{M}$

**Table 1.** Condensability of different DNA lengths and GC-content by spermine.

The increased spermine-induced condensability of AT-rich DNA relative to GC-rich DNA confirms what was predicted from all-atom molecular dynamics simulations and was experimentally validated previously using single-molecule FRET quantification of the frequency of transient contacts between two double stranded DNA molecules trapped inside a single vesicle [28]. As we increase the length of DNA from 70 bp to 230 bp, the threshold concentration of spermine for DNA condensation decreased from 50  $\mu$ M to 10  $\mu$ M (Table 1), indicating that DNA condensation by spermine depends on the availability of locations for spermine to associate with.

In order to further expand this study toward condensation in the chromatin context, we generated a mono-nucleosome construct containing a 147 bp 601 nucleosome positioning sequence (denoted as N) flanked by an 80 bp linker containing biotin and a 3 bp linker containing Cy5 wrapped around a histone octamer with a Cy3 labeled H2A histone (Fig 2B). This ‘80N3’ nucleosome construct displays the same apparent two-dimensional diffusional behavior as naked DNA of the same length and forms bright, immobile condensates similar to definite condensation of DNA observed upon 100 mM spermine addition (Fig 2B). Using both 230 bp long DNA and 80N3 nucleosomes we then tested several known and suspected condensing agents and determined the concentrations required to initiate condensation (Fig 2A, Table 2). Spermine and spermidine were both previously described to drive DNA condensation via electrostatic interactions with DNA [40]. We found that these

polyamines behaved similarly when condensing DNA and 80N3 (Fig 2B, Table 2); however, DNA required a lower concentration of spermine to initiate condensation than nucleosomes while requiring a higher spermidine concentration to form initial condensates than nucleosomes (Table 2).

	43N43 DNA	80N3 Nucleosome
Spermine (4+)	10 $\mu$ M	20 $\mu$ M
Spermidine (3+)	30 $\mu$ M	20 $\mu$ M
Putrescine (2+)	>1M	>1M
HP1 $\alpha$	10 nM	50 nM
Ki-67	1 nM	100 pM

**Table 2. Condensing agent concentrations required to initiate DNA or nucleosome condensation on a 2D platform.**

Interestingly, spermidine forms larger, more complex DNA condensates than spermine at the same concentration, 100 mM, (Fig 2C, 2D). We also used the +2 charged polyamine putrescine and found that this was not sufficient to drive DNA condensation on the SBL

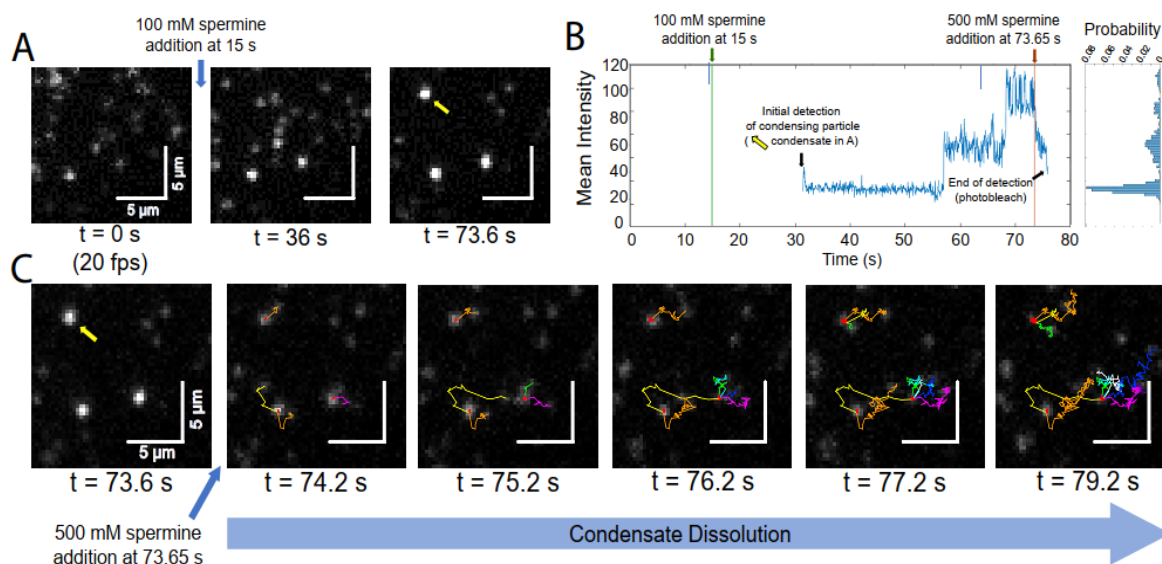


**Figure 3.** Realtime tracking of single molecules during condensation and decondensation: (A) snapshots highlighting condensate formation after the addition of 100 mM spermine. (B) Fluorescence intensity profile of a nucleating particle (denoted by a yellow arrow in A) during the inclusion of additional particles into the condensate. (C) Snapshots highlighting condensate dissolution after the addition of 500 mM spermine to the SLB in A. New particle trajectories are given a different color.

even up to 1 M. We also tested HP1 $\alpha$ , which binds to H3K9 methylated histones and promotes the formation of heterochromatin via recruitment of remodelers or binding partners [3]. We found that 5-fold more concentrated HP1 $\alpha$  was required to initially drive 80N3 nucleosome condensation than DNA condensation, which occurred at HP1 $\alpha$  concentrations as low as 10 nM (Table 2). Definitive condensation by HP1 $\alpha$  occurred at 150 nM for DNA and at 200 nM for 80N3 nucleosomes (Supplemental Figure 2). Since HP1 $\alpha$  has a DNA binding motif [41], our studies further support the idea that improved DNA accessibility leads to improved condensation. We also note that HP1 $\alpha$ -

mediated nucleosome condensation occurred even in the absence of H3K9 methylation.

3.2 Macromolecular condensation events can be visualized at the single molecule level in real time

Our SLB single molecule imaging platform also allows us to visualize DNA and nucleosome condensation in real time. Single particles were tracked in order to determine their mean-squared displacement (MSD) and subsequently, their diffusion coefficients. Cy3-labeled dsDNA bound to the SLB surface had an average diffusion coefficient of  $0.49 \pm 0.019 \mu\text{m}^2/\text{s}$  with a lower limit of  $0.001 \mu\text{m}^2/\text{s}$  (Fig 1E). Single particle diffusion coefficients were

measured before and after the addition of spermine and a clear shift from a high-mobility state to a low or no-mobility state was observed, from an average of  $0.49 \pm 0.019 \mu\text{m}^2/\text{s}$  to  $0.17 \pm 0.019 \mu\text{m}^2/\text{s}$ , with a shift back to  $0.48 \pm 0.025 \mu\text{m}^2/\text{s}$  after the dispersal caused by spermine-mediated charge inversion (Fig 1E). A similar shift in diffusion coefficients was seen when subjecting 80N3 nucleosomes to the same spermine-mediated condensation, from an average of  $0.94 \pm 0.05 \mu\text{m}^2/\text{s}$  to  $0.17 \pm 0.019 \mu\text{m}^2/\text{s}$  (Fig 2E). The same condensate formation and dispersal pattern was not seen, however, when performing the same experiments on fluorescent particles that do not form condensates such 7% of a rhodamine-labeled phospholipid (Fig 2F). We carried out real-time single molecule experiments to visualize condensate formation and dissolution as the condensing agents are added via flow with a syringe pump (Fig 3A). Once the condensates were fully formed, 500 mM spermine was added to promote condensate dispersal (Fig 3C) where we can see particles leave condensates and interact with other particles from dispersing condensates (Video 1, Fig 3C orange trace) or other condensates themselves (Video 1, Fig 3C yellow trace). From these videos, we were able to track the individual particles as they entered condensates by labeling each particle and observing their trajectories. We can then theoretically count the number of particles in a condensate by measuring the stepwise increase in intensity (Fig 3B) However, transient particle-particle interactions of condensate-forming particles coupled with photobleaching lead to unreliable particle-per-condensate counts using intensity alone and must therefore be coupled with another metric for condensate identification.

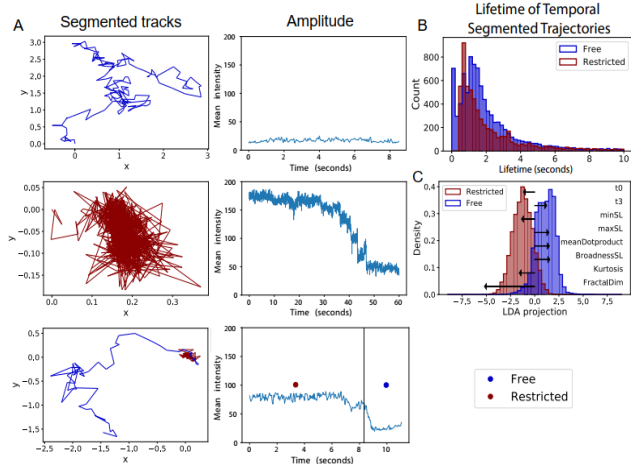
The large full width half maximum (FWHM) of the diffusion coefficient histograms seen in diffusing particles (Fig 1E, 2E blue histograms) indicates that the particles tend to have varying diffusion coefficients, which can also be visualized through direct observation (Video 2) and highlights the multiple diffusion modes observed within a population of SLB bound particles. To better track and categorize individual particles and their time-dependent diffusional behavior as they participate in condensation, we utilized a rolling MSD analysis in conjunction with a machine-learning algorithm termed diffusional fingerprinting [29]. From this analysis, we were able to categorize trajectories into subsegments of either a restricted or free movement state (Fig 4A) and determine which diffusional state a particle spends the most time in (Fig 4B) and its specific diffusional metrics (Fig 4C). In addition, we applied a fluorescence intensity analysis in order to observe a stepwise intensity increase during particle inclusion into condensates (Fig 4A, 3B). From this diffusional fingerprinting analysis, we found and ranked the key distinct trajectory metrics that discriminate restricted movement,

**Figure 4.** Diffusional fingerprinting of particles before and during condensation/ decondensation: (A) Temporally segmented traces by rolling MSD analysis with their respective intensity profile. Showing a representative free moving trace, restricted trace and a heterogenous diffusing trace. Intensity profiles show that the free moving tracks have a generally constant intensity amplitude while the restricted trajectory has an intensity profile indicative of condensate disassembly. (B) The lifetime of free and restricted segments. (C) shows a linear discriminate analysis dimensionality reduced representation of the diffusional fingerprints of free and restricted trajectory segments with the top 8 diffusional metrics separating the two distributions shown as black arrows.

characteristic of condensates, from free moving particles using a linear discriminate analysis (LDA) dimensionality reduction. Using LDA, we found that the fractal dimension of trajectories was the most important metric distinguishing restricted from non-restricted movements (Fig 4C). In addition, trajectory step length distribution, the span of distances particles travel in a frame, and kurtosis, a measure of distribution ‘tailed-ness’, both play important roles in identifying condensing particles (Fig 4C). In addition, 5 other metrics were used to discriminate diffusion behaviors: residence time in the state with the lowest ( $t_0$ ) or highest ( $t_3$ ) diffusion coefficient (four total diffusional states analyzed by Hidden Markov Model), minimum step length, maximum step length, and the mean dot product of a particle’s trajectory, a measure of persistence in trajectory directionality (Fig 4C). When comparing diffusion characteristics of DNA alone vs DNA incubated with spermine for 60 seconds, 28% of trajectories in the absence of spermine had more than one diffusion state vs 43% of trajectories in the presence of spermine (Table 3), likely due to particle inclusion into condensates. With the temporal segmentation and diffusional fingerprinting, potential condensate diffusion and free movement seem linearly separable, and together with intensity profile analysis, serve to map condensate assembly and disassembly mechanisms (Fig 4).

### 3.3 Nucleosome condensation driven by Ki-67

At the onset of mitosis, Ki-67 is one of the earliest proteins to associate with the perichromosomal layer, a ribonucleoprotein coating on mitotic chromosomes [30]. Ki-67 has a high net positive electrostatic charge which serves to prevent mitotic chromosomes from collapsing into an inseparable multi-chromosome mass upon nuclear envelope disassembly and helps maintain chromosome individuality and motility during mitosis [30, 42]. With evidence highlighting the chromosomal surfactant behavior of Ki-67 [31] we wanted to investigate if Ki-67 could serve as a nucleosome condensing agent. To this end we titrated full length Ki-67 onto an SLB bound with 80N3 nucleosomes and found that full length Ki-67 at 300 pM concentration can initiate the condensation of these nucleosomes (Fig 5A), a concentration much lower than what has so far been seen with other condensing agents tested in this study (Table 2). Before condensation by Ki-67 the average diffusion coefficient of SLB-bound nucleosomes was  $0.13 \pm 0.008 \mu\text{m}^2/\text{s}$  with a downward shift to  $0.009 \pm 0.0005 \mu\text{m}^2/\text{s}$  after the addition of 300 pM Ki-67 (Table 2, bottom row).



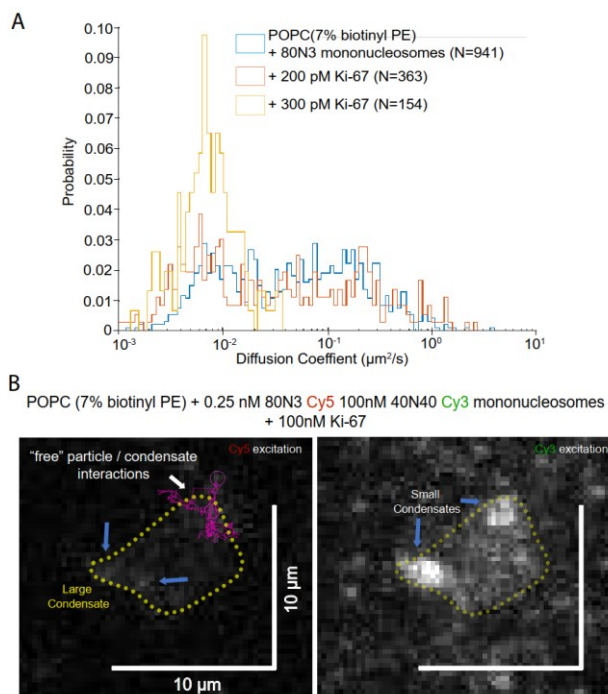


**Figure 5.** (A) Overlay of diffusion histograms obtained from tracked particles after the addition of 200pM, and 300pM Ki-67, (B) Large condensate sparsely labelled with Cy5 40N40 nucleosomes in a background of Cy3 labeled 80N3 nucleosomes. Condensate is outlined with a yellow dotted line and the trajectory of an interacting particle highlighted in magenta. Intermediate sized immobile condensates are shown using blue arrows.

To investigate particle dynamics within Ki-67 condensates, we performed a sparse labelling experiment with 0.25 nM Cy5 labelled 80N3 nucleosomes and 100 nM Cy3 labelled 40N40 nucleosomes bound to an SLB. The high concentration of nucleosomes allowed for the formation of large condensates that can be observed with Cy3 while the low concentration of Cy5 labelled nucleosomes allows for the tracking of particles within the Cy3-verified condensates (Fig 5B). Colocalized with these large condensates is a significant proportion of particles that are stationary as well as dense immobile condensates seen both by Cy3 and by sparsely labelled Cy5 (Fig 5B, blue arrows) which implies that these large loosely-packed condensates are composed of a network of the smaller, bright, dense condensates (Fig 2D, 5B) reminiscent of the dense bright condensates seen in previous experiments (Fig 2C). Visually, large condensates appear to take on a multitude of shapes but are immobile and seldom form circular condensates like what is often expected of LLPS. Despite

	Has >1 Diffusional State	Has >2 Diffusional State	Has >1 Diffusional State ends restricted	Only restricted entire life
Pre-condensation	28 %	14%	15%	16%
Post-condensation	43%	25%	22%	28%
Concurrent condensation & dissolution	23%	13%	10%	9%

**Table 3: Diffusional characteristics of DNA before inducing condensation, after condensation is induced, and when condensation and dissolution are initiated in the same video. Obtained from dimensional fingerprinting analysis.**

this, the presence of particles capable of associating with, dissociating from, and travelling within or through a Ki-67 condensate would indicate that these large condensates have partial-fluid like properties (Fig 5B). Of the 6 observed “loosely-packed” condensates where sparsely labelled particles have a greater than 2 second lifetime, 5 condensates are seen interacting with external particles. Tracking shows that particles can “bounce” along the edge of a condensate, enter the condensate, move within the condensate in a confined manner, or all three behaviors in a single trajectory (Fig 5B). Ki-67 condensates were not directly observed fusing to form larger condensates.

#### 4. CONCLUSIONS

In this work, we have used supported lipid bilayers as a platform for visualizing the 2-dimensional diffusion of surface-bound macromolecules such as DNA and nucleosomes with different condensing agents. We then observed that the threshold concentration of condensing agents depends on the length and GC content of the DNA, where longer length and lower GC contents led to initial condensation at lower condensing agent concentrations. Furthermore, DNA condensation by spermine can be reversed upon the addition of a DNA saturating concentration of spermine, highlighting that the condensation does not perturb the SLB and allows for the observation of condensation and dissolution reversibly. We then used SLBs in tandem with total internal reflection fluorescence

microscopy for visualizing real time condensation and dispersal of condensates which allows tracking of individual particles entering and exiting condensates. These particle tracking data imply the presence of multiple diffusion states as indicated by the wide range of diffusion coefficients of DNA in the absence of condensing agents. Using diffusional fingerprinting and temporal segmentation of diffusion we confirmed the existence of multiple diffusional states in DNA trajectories, namely a mobile and immobile state and identified their most discriminative diffusional characteristics. Together, temporal segmentation and diffusional fingerprinting can map diffusional transitions and diffusional features which may, going forward, allow us to track and identify condensing particles from diffusion behavior alone. We aim to use this in future experiments to analyze the kinetic behavior of suspected condensing agents.

We expanded this study by investigating the condensing behavior of nucleosomes in the presence of several known and suspected condensing agents. Amongst these condensing agents we chose to take a closer look at the protein Ki-67, a proposed chromosomal surfactant which led to the robust formation of nucleosome condensates at concentrations lower than any other condensing agent examined in this study. To investigate particle behavior in Ki-67 condensates, we applied Ki-67 to high density of nucleosomes that are sparsely labeled and observed that large condensates may be

formed by a semi-permeable network of smaller, dense condensates.

Many proteins that participate in LLPS achieve condensation through multivalent interactions, where particles with a valency of 2 cannot form space-spanning interacting networks without linking to higher valence molecules [32]. With evidence that full length Ki-67 is capable of nucleosome condensation, it stands to reason that multiple motifs are likely responsible for Ki-67 condensation. To this end, future directions involve testing the nucleosome condensability by individual Ki-67 motifs as well as investigating the impact of dephosphorylated Ki-67 [30] on nucleosome condensation. Overall, this study serves to highlight the utility of SLBs as a tool for studying real-time kinetics of nucleosome condensation and condensate dispersal, which can be further expanded to investigate other systems such as signal transducing biomolecular condensates that form as a result of membrane receptors binding their ligands [33].

## ASSOCIATED CONTENT

**Supporting Information.** Widefield Images depicting the fluorescence recovery after photobleaching (FRAP) of supported lipid bilayers as they are either bound by a macromolecule or not, oTIRF images highlighting the initial condensation of DNA and nucleosomes by HP1

## AUTHOR INFORMATION

### Corresponding Author

\* **Taekjip Ha** - Department of Biophysics and Biophysical Chemistry, Johns Hopkins University School of Medicine, Baltimore, MD 21205, USA

-Department of Biophysics, Johns Hopkins University, Baltimore, MD 21218, USA

-Department of Biomedical Engineering, Johns Hopkins University, Baltimore, MD 21218, USA

-Howard Hughes Medical Institute, Baltimore, MD 21205, USA

<https://orcid.org/0000-0003-2195-6258>; email: tjha@jhu.edu

### Authors

**Nils Benning** - Department of Cellular biology, Molecular biology, Developmental biology, and Biophysics, Johns Hopkins University, Baltimore, MD 21218, USA

**Jacob Kaestel-Hansen** - Department of Chemistry and Nanoscience Centre, University of Copenhagen, Copenhagen, Denmark

**Fahad Rashid** - Department of Biophysics and Biophysical Chemistry, Johns Hopkins University School of Medicine, Baltimore, MD 21205, USA

**Sangwoo Park** - Department of Biophysics and Biophysical Chemistry, Johns Hopkins University School of Medicine, Baltimore, MD 21205, USA

**Raquel Merino Urteaga** - Department of Cellular biology, Molecular biology, Developmental biology, and Biophysics, Johns Hopkins University, Baltimore, MD 21218, USA

**Ting-Wei Liao** - Department of Biophysics and Biophysical Chemistry, Johns Hopkins University School of Medicine, Baltimore, MD 21205, USA

**Jingzhou Hao** - Department of Biophysics and Biophysical Chemistry, Johns Hopkins University School of Medicine, Baltimore, MD 21205, USA

**James M. Berger** - Department of Biophysics and Biophysical Chemistry, Johns Hopkins University School of Medicine, Baltimore, MD 21205, USA

**Nikos S. Hatzakis** - Department of Chemistry and Nanoscience Centre, University of Copenhagen, Copenhagen, Denmark

-Novo Nordisk Foundation Centre for Protein Research, Faculty of Health and Medical Sciences, University of Copenhagen, Copenhagen, Denmark

## Author Contributions

All authors have given approval to the final version of the manuscript.

## Funding Sources

This work was supported by the National Institutes of Health (GM122569 to T.H), NSF EFMA (1933303), The Villum Foundation (BioNEC 18333 & Villum experiment grant 40801), and The Novo Nordisk Foundation (NNF14CC0001).

## ACKNOWLEDGMENT

The authors thank Dr. Matthew Poyton and Claudia Carcamo for their initial instruction on the formation and handling of supported lipids bilayers. This work was supported by the National Institutes of Health (GM122569 to T.H), NSF EFMA (1933303), The Villum Foundation (BioNEC 18333 & Villum experiment grant 40801), and The Novo Nordisk Foundation (NNF14CC0001). The authors wish to thank The Histone Source at Colorado State University for generating the *Xenopus* histone octamers used in this study

## ABBREVIATIONS

LLPS, liquid-liquid phase separation; SLB, supported lipid bilayer; SUV, small unilamellar vesicle; TIRM, total internal reflection microscopy; TIRF, total internal reflection fluorescence; MSD, mean squared displacement; LAP, linear assignment problem; LoG, Laplacian of Gaussian; FRAP, fluorescence recovery after photobleaching; LDA, linear discriminate analysis; FRET, fluorescence resonance energy transfer; FWHM, full width half maximum;

## REFERENCES

- [1] Minois, Nadège, Didac Carmona-Gutierrez, and Frank Madeo. "Polyamines in Aging and Disease." *Aging* 3, no. 8 (n.d.): 716–32. <https://doi.org/10.18632/aging.100361>.
- [2] Harami, Gábor M., Zoltán J. Kovács, Rita Pancsa, János Pálkás, Veronika Baráth, Krisztián Tárnok, András Málnási-Csizmadia, and Mihály Kovács. "Phase Separation by SsDNA Binding Protein Controlled via Protein–protein and Protein–DNA Interactions." *Proceedings of the National Academy of Sciences* 117, no. 42 (October 20, 2020): 26206–17. <https://doi.org/10.1073/pnas.2000761117>.
- [3] Larson, Adam G., Daniel Elnatan, Madeline M. Keenen, Michael J. Trnka, Jonathan B. Johnston, Alma L. Burlingame, David A. Agard, Sy Redding, and Geeta J. Narlikar. "Liquid Droplet Formation by HP1 $\alpha$  Suggests a Role for Phase Separation in Heterochromatin." *Nature* 547, no. 7662 (July 1, 2017): 236–40. <https://doi.org/10.1038/nature22822>.
- [4] Feric, Marina, Nilesh Vaidya, Tyler S. Harmon, Diana M. Mitrea, Lian Zhu, Tiffany M. Richardson, Richard W. Kriwacki, Rohit V. Pappu, and Clifford P. Brangwynne. "Coexisting Liquid Phases Underlie Nucleolar Subcompartments." *Cell* 165, no. 7 (June 16, 2016): 1686–97. <https://doi.org/10.1016/j.cell.2016.04.047>.
- [5] Wang, Bin, Lei Zhang, Tong Dai, Ziran Qin, Huasong Lu, Long Zhang, and Fangfang Zhou. "Liquid–Liquid Phase Separation in Human Health and Diseases." *Signal Transduction and Targeted Therapy* 6, no. 1 (August 2, 2021): 290. <https://doi.org/10.1038/s41392-021-00678-1>.
- [6] Li, Yun R., Oliver D. King, James Shorter, and Aaron D. Gitler. "Stress Granules as Crucibles of ALS Pathogenesis."

*Journal of Cell Biology* 201, no. 3 (April 29, 2013): 361–72. <https://doi.org/10.1083/jcb.201302044>.

[7] Polymenidou, Magdalini, and Don W. Cleveland. “The Seeds of Neurodegeneration: Prion-like Spreading in ALS.” *Cell* 147, no. 3 (October 28, 2011): 498–508. <https://doi.org/10.1016/j.cell.2011.10.011>.

[8] Patel, Avinash, Hyun O. Lee, Louise Jawerth, Shovamayee Maharana, Marcus Jahnel, Marco Y. Hein, Stoyno Stoynov, et al. “A Liquid-to-Solid Phase Transition of the ALS Protein FUS Accelerated by Disease Mutation.” *Cell* 162, no. 5 (August 27, 2015): 1066–77. <https://doi.org/10.1016/j.cell.2015.07.047>.

[9] Schmidt, Hermann Broder, Ariana Barreau, and Rajat Rohatgi. “Phase Separation-Deficient TDP43 Remains Functional in Splicing.” *Nature Communications* 10, no. 1 (October 25, 2019): 4890. <https://doi.org/10.1038/s41467-019-12740-2>.

[10] Ray, Soumik, Nitu Singh, Rakesh Kumar, Komal Patel, Satyaprakash Pandey, Debalina Datta, Jaladhar Mahato, et al. “ $\alpha$ -Synuclein Aggregation Nucleates through Liquid–Liquid Phase Separation.” *Nature Chemistry* 12, no. 8 (August 1, 2020): 705–16. <https://doi.org/10.1038/s41557-020-0465-9>.

[11] Ambadipudi, Susmitha, Jacek Biernat, Dietmar Riedel, Eckhard Mandelkow, and Markus Zweckstetter. “Liquid–Liquid Phase Separation of the Microtubule-Binding Repeats of the Alzheimer-Related Protein Tau.” *Nature Communications* 8, no. 1 (August 17, 2017): 275. <https://doi.org/10.1038/s41467-017-00480-0>.

[12] Zbinden, Aurélie, Manuela Pérez-Berlanga, Pierre De Rossi, and Magdalini Polymenidou. “Phase Separation and Neurodegenerative Diseases: A Disturbance in the Force.” *Developmental Cell* 55, no. 1 (October 12, 2020): 45–68. <https://doi.org/10.1016/j.devcel.2020.09.014>.

[13] Perdikari, Theodora Myrto, Anastasia C Murthy, Veronica H Ryan, Scott Watters, Mandar T Naik, and Nicolas L Fawzi. “SARS-CoV-2 Nucleocapsid Protein Phase-Separates with RNA and with Human hnRNPs.” *The EMBO Journal* 39, no. 24 (December 15, 2020): e106478. <https://doi.org/10.15252/embj.2020106478>.

[14] Wang, Jia, Chengrui Shi, Qun Xu, and Hang Yin. “SARS-CoV-2 Nucleocapsid Protein Undergoes Liquid–Liquid Phase Separation into Stress Granules through Its N-Terminal Intrinsically Disordered Region.” *Cell Discovery* 7, no. 1 (January 21, 2021): 5. <https://doi.org/10.1038/s41421-020-00240-3>.

[15] Heinrich Bianca S., Maliga Zoltan, Stein David A., Hyman Anthony A., Whelan Sean P. J., and Palese Peter. “Phase Transitions Drive the Formation of Vesicular Stomatitis Virus Replication Compartments.” *MBio* 9, no. 5 (September 4, 2018): e02290-17. <https://doi.org/10.1128/mBio.02290-17>.

[16] Sanders, David W., Nancy Kedersha, Daniel S.W. Lee, Amy R. Strom, Victoria Drake, Joshua A. Riback, Dan Bracha, et al. “Competing Protein-RNA Interaction Networks Control Multi-phase Intracellular Organization.” *Cell* 181, no. 2 (April 16, 2020): 306–324.e28. <https://doi.org/10.1016/j.cell.2020.03.050>.

[17] Leslie, Mitch. “Separation Anxiety” *Science* (January 21, 2021) doi: 10.1126/science.abg6495

[18] Gitler, Aaron D., James Shorter, Taekjip Ha, and Sua Myong. “Just Took a DNA Test, Turns Out 100% Not That Phase.” *Molecular Cell* 78, no. 2 (April 16, 2020): 193–94. <https://doi.org/10.1016/j.molcel.2020.03.029>.

[19] Bracha, Dan, Mackenzie T. Walls, Ming-Tzo Wei, Lian Zhu, Martin Kurian, José L. Avalos, Jared E. Toettcher, and Clifford P. Brangwynne. “Mapping Local and Global Liquid Phase Behavior in Living Cells Using Photo-Oligomerizable Seeds.” *Cell* 175, no. 6 (November 29, 2018): 1467–1480.e13. <https://doi.org/10.1016/j.cell.2018.10.048>.

[20] Jan Akhuzada, Muhammad, Francesca D’Autilia, Balasubramanian Chandramouli, Nicholas Bhattacharjee, Andrea Catte, Roberto Di Rienzo, Francesco Cardarelli, and Giuseppe

Brancato. “Interplay between Lipid Lateral Diffusion, Dye Concentration and Membrane Permeability Unveiled by a Combined Spectroscopic and Computational Study of a Model Lipid Bilayer.” *Scientific Reports* 9, no. 1 (February 6, 2019): 1508. <https://doi.org/10.1038/s41598-018-37814-x>.

[21] Koch, Sabrina, Anne-Bart Seinen, Michael Kamel, Daniel Kuckla, Cornelia Monzel, Alexej Kedrov, and Arnold J.M. Driesen. “Single-Molecule Analysis of Dynamics and Interactions of the SecYEG Translocon.” *The FEBS Journal* 288, no. 7 (April 1, 2021): 2203–21. <https://doi.org/10.1111/febs.15596>.

[22] Kudalkar, E. M., Davis, T. N., & Asbury, C. L. “Single-Molecule Total Internal Reflection Fluorescence Microscopy.” *Cold Spring Harbor protocols*, no. 5 (May 2, 2016) <https://doi.org/10.1101/pdb.top077800>

[23] Johnson, Joseph M., Taekjip Ha, Steve Chu, and Steven G. Boxer. “Early Steps of Supported Bilayer Formation Probed by Single Vesicle Fluorescence Assays.” *Biophysical Journal* 83, no. 6 (December 1, 2002): 3371–79. [https://doi.org/10.1016/S0006-3495\(02\)75337-X](https://doi.org/10.1016/S0006-3495(02)75337-X).

[24] Perez TD, Nelson WJ, Boxer SG, Kam L. “E-cadherin tethered to micropatterned supported lipid bilayers as a model for cell adhesion.” *Langmuir*. 25 no. 21 (December 6. 2005): 11963–11968. doi:10.1021/la052264a

[25] Grusky, Dashiell S., Frank R. Moss, and Steven G. Boxer. “Recombination between  $^{13}\text{C}$  and  $^2\text{H}$  to Form Acetylide ( $^{13}\text{C}^{22}\text{H}$ ) Probes Nanoscale Interactions in Lipid Bilayers via Dynamic Secondary Ion Mass Spectrometry: Cholesterol and GM1 Clustering.” *Analytical Chemistry* 94, no. 27 (July 12, 2022): 9750–57. <https://doi.org/10.1021/acs.analchem.2c01336>.

[26] Tinevez, Jean-Yves, Nick Perry, Johannes Schindelin, Genevieve M. Hoopes, Gregory D. Reynolds, Emmanuel Laplantine, Sebastian Y. Bednarek, Spencer L. Shorte, and Kevin W. Eliceiri. “TrackMate: An Open and Extensible Platform for Single-Particle Tracking.” *Image Processing for Biologists* 115 (February 15, 2017): 80–90. <https://doi.org/10.1016/j.ymeth.2016.09.016>.

[27] Banjade, Sudeep, and Michael K Rosen. “Phase Transitions of Multivalent Proteins Can Promote Clustering of Membrane Receptors.” Edited by Anthony A Hyman. *ELife* 3 (October 16, 2014): e04123. <https://doi.org/10.7554/eLife.04123>.

[28] Yoo, Jehoong, Hajin Kim, Aleksei Aksimentiev, and Taekjip Ha. “Direct Evidence for Sequence-Dependent Attraction between Double-Stranded DNA Controlled by Methylation.” *Nature Communications* 7, no. 1 (March 22, 2016): 11045. <https://doi.org/10.1038/ncomms11045>.

[29] Pinholt, Henrik D., Søren S.-R. Bohr, Josephine F. Iversen, Wouter Boomsma, and Nikos S. Hatzakis. “Single-Particle Diffusional Fingerprinting: A Machine-Learning Framework for Quantitative Analysis of Heterogeneous Diffusion.” *Proceedings of the National Academy of Sciences* 118, no. 31 (August 3, 2021): e2104624118. <https://doi.org/10.1073/pnas.2104624118>.

[30] Sun, Xiaoming, and Paul D. Kaufman. “Ki-67: More than a Proliferation Marker.” *Chromosoma* 127, no. 2 (June 1, 2018): 175–86. <https://doi.org/10.1007/s00412-018-0659-8>.

[31] Cuylen-Haering, Sara, Mina Petrovic, Alberto Hernandez-Armandariz, Maximilian W. G. Schneider, Matthias Samwer, Claudia Blaukopf, Liam J. Holt, and Daniel W. Gerlich. “Chromosome Clustering by Ki-67 Excludes Cytoplasm during Nuclear Assembly.” *Nature* 587, no. 7833 (November 1, 2020): 285–90. <https://doi.org/10.1038/s41586-020-2672-3>.

[32] Sanders, David W., Nancy Kedersha, Daniel S.W. Lee, Amy R. Strom, Victoria Drake, Joshua A. Riback, Dan Bracha, et al. “Competing Protein-RNA Interaction Networks Control Multi-phase Intracellular Organization.” *Cell* 181, no. 2 (April 16, 2020): 306–324.e28. <https://doi.org/10.1016/j.cell.2020.03.050>.

[33] Jaqaman, Khuloud, and Jonathon A. Ditlev. “Biomolecular Condensates in Membrane Receptor Signaling.” *Cell Signalling*

69 (April 1, 2021): 48–54.

<https://doi.org/10.1016/j.ceb.2020.12.006>.

[34] Strom, Amy R., Alexander V. Emelyanov, Mustafa Mir, Dmitry V. Fyodorov, Xavier Darzacq, and Gary H. Karpen. “Phase Separation Drives Heterochromatin Domain Formation.” *Nature* 547, no. 7662 (July 1, 2017): 241–45. <https://doi.org/10.1038/nature22989>.

[35] Hilbert, Lennart, Yuko Sato, Ksenia Kuznetsova, Tommaso Bianucci, Hiroshi Kimura, Frank Jülicher, Alf Honigsmann, Vasily Zaburdaev, and Nadine L. Vastenhouw. “Transcription Organizes Euchromatin via Microphase Separation.” *Nature Communications* 12, no. 1 (March 1, 2021): 1360. <https://doi.org/10.1038/s41467-021-21589-3>.

[36] Strickfaden, Hilmar, Thomas O. Tolsma, Ajit Sharma, D. Alan Underhill, Jeffrey C. Hansen, and Michael J. Hendzel. “Condensed Chromatin Behaves like a Solid on the Mesoscale In Vitro and in Living Cells.” *Cell* 183, no. 7 (December 23, 2020): 1772–1784.e13. <https://doi.org/10.1016/j.cell.2020.11.027>.

[37] Rafiee, Mahmoud-Reza, Julian A Zagalak, Sviatoslav Sidorov, Sebastian Steinhäuser, Karen Davey, Jernej Ule, and Nicholas M Luscombe. “Chromatin-Contact Atlas Reveals Disorder-Mediated Protein Interactions and Moonlighting Chromatin-Associated RBPs.” *Nucleic Acids Research* 49, no. 22 (December 16, 2021): 13092–107. <https://doi.org/10.1093/nar/gkab1180>.

[38] Zhang, Lei, Xinran Geng, Fangfang Wang, Jinshan Tang, Yu Ichida, Arishya Sharma, Sora Jin, et al. “53BP1 Regulates Heterochromatin through Liquid Phase Separation.” *Nature Communications* 13, no. 1 (January 18, 2022): 360. <https://doi.org/10.1038/s41467-022-28019-y>.

[39] Quinodoz, Sofia A., Joanna W. Jachowicz, Prashant Bhat, Noah Ollikainen, Abhik K. Banerjee, Isabel N. Goronzy, Mario R. Blanco, et al. “RNA Promotes the Formation of Spatial Compartments in the Nucleus.” *Cell* 184, no. 23 (November 11, 2021): 5775–5790.e30. <https://doi.org/10.1016/j.cell.2021.10.014>.

[40] Childs, A. C., D. J. Mehta, and E. W. Gerner. “Polyamine-Dependent Gene Expression.” *Cellular and Molecular Life Sciences CMLS* 60, no. 7 (July 1, 2003): 1394–1406. <https://doi.org/10.1007/s00018-003-2332-4>.

[41] Kumar, Amarjeet, and Hidetoshi Kono. “Heterochromatin Protein 1 (HP1): Interactions with Itself and Chromatin Components.” *Biophysical Reviews* 12, no. 2 (April 1, 2020): 387–400. <https://doi.org/10.1007/s12551-020-00663-y>.

[42] Cuylen, Sara, Claudia Blaukopf, Antonio Z. Politi, Thomas Müller-Reichert, Beate Neumann, Ina Poser, Jan Ellenberg, Anthony A. Hyman, and Daniel W. Gerlich. “Ki-67 Acts as a Biological Surfactant to Disperse Mitotic Chromosomes.” *Nature* 535, no. 7611 (July 1, 2016): 308–12. <https://doi.org/10.1038/nature18610>.

[43] Raspau, E., I. Chaperon, A. Leforestier, and F. Livolant. “Spermine-Induced Aggregation of DNA, Nucleosome, and Chromatin.” *Biophysical Journal* 77, no. 3 (September 1, 1999): 1547–55. [https://doi.org/10.1016/S0006-3495\(99\)77002-5](https://doi.org/10.1016/S0006-3495(99)77002-5).

[44] Keenen, Madeline M, David Brown, Lucy D Brennan, Roman Renger, Harrison Khoo, Christopher R Carlson, Bo Huang, Stephan W Grill, Geeta J Narlikar, and Sy Redding. “HP1

Proteins Compact DNA into Mechanically and Positionally Stable Phase Separated Domains.” Edited by Sebastian Deindl and Kevin Struhl. *ELife* 10 (March 4, 2021): e64563.

<https://doi.org/10.7554/eLife.64563>.

[45] Strom, Amy R, Ronald J Biggs, Edward J Banigan, Xiaotao Wang, Katherine Chiu, Cameron Herman, Jimena Collado, et al. “HP1 $\alpha$  Is a Chromatin Crosslinker That Controls Nuclear and Mitotic Chromosome Mechanics.” Edited by Geeta J Narlikar, Kevin Struhl, and Sy Redding. *ELife* 10 (June 9, 2021): e63972. <https://doi.org/10.7554/eLife.63972>.

[46] Machida, Shinichi, Yoshimasa Takizawa, Masakazu Ishimaru, Yukihiko Sugita, Satoshi Sekine, Jun-ichi Nakayama, Matthias Wolf, and Hitoshi Kurumizaka. “Structural Basis of Heterochromatin Formation by Human HP1.” *Molecular Cell* 69, no. 3 (February 1, 2018): 385–397.e8. <https://doi.org/10.1016/j.molcel.2017.12.011>.

[47] Chan, Yee-Hung M, and Steven G Boxer. “Model Membrane Systems and Their Applications.” *Model Systems/Biopolymers* 11, no. 6 (December 1, 2007): 581–87. <https://doi.org/10.1016/j.cbpa.2007.09.020>.

[48] Lengerich, Bettina van, Robert J. Rawle, and Steven G. Boxer. “Covalent Attachment of Lipid Vesicles to a Fluid-Supported Bilayer Allows Observation of DNA-Mediated Vesicle Interactions.” *Langmuir* 26, no. 11 (June 1, 2010): 8666–72. <https://doi.org/10.1021/la904822f>.

[49] Chung, Minsub, and Steven G. Boxer. “Stability of DNA-Tethered Lipid Membranes with Mobile Tethers.” *Langmuir* 27, no. 9 (May 3, 2011): 5492–97. <https://doi.org/10.1021/la200234h>.

[50] Larson, Adam G., Daniel Elnatan, Madeline M. Keenen, Michael J. Trnka, Jonathan B. Johnston, Alma L. Burlingame, David A. Agard, Sy Redding, and Geeta J. Narlikar. “Liquid Droplet Formation by HP1 $\alpha$  Suggests a Role for Phase Separation in Heterochromatin.” *Nature* 547, no. 7662 (July 1, 2017): 236–40. <https://doi.org/10.1038/nature22822>.

[51] Luger, Karolin, Thomas J. Rechsteiner, and Timothy J. Richmond. “Expression and Purification of Recombinant Histones and Nucleosome Reconstitution.” In *Chromatin Protocols*, edited by Peter B. Becker, 1–16. Totowa, NJ: Humana Press, 1999. <https://doi.org/10.1385/1-59259-681-9:1>.

[52] Wei, Ming-Tzo, Shana Elbaum-Garfinkle, Alex S. Holehouse, Carlos Chih-Hsiung Chen, Marina Feric, Craig B. Arnold, Rodney D. Priestley, Rohit V. Pappu, and Clifford P. Brangwynne. “Phase Behaviour of Disordered Proteins Underlying Low Density and High Permeability of Liquid Organelles.” *Nature Chemistry* 9, no. 11 (November 1, 2017): 1118–25. <https://doi.org/10.1038/nchem.2803>.

[53] Kamagata, Kiyoto, Nanako Iwaki, Milan Kumar Hazra, Saori Kanbayashi, Trishit Banerjee, Rika Chiba, Seiji Sakamoto, et al. “Molecular Principles of Recruitment and Dynamics of Guest Proteins in Liquid Droplets.” *Scientific Reports* 11, no. 1 (September 29, 2021): 19323. <https://doi.org/10.1038/s41598-021-98955-0>.